Reflective SFT-FBG Hybrid Micro-Probe for Simultaneous Measurement of Relative Humidity and Temperature

Zhankun Lv, Panpan Niu, Junfeng Jiang, Shuang Wang, Yize Liu, and Tiegen Liu

***Abstract*—An optical fiber probe composed of a fiber Bragg grating (FBG) and a reflective S fiber taper (SFT) with graphene oxide (GO) film, for simultaneous relative humidity (RH) and temperature measurement, was proposed and experimentally demonstrated in this paper. The SFT is made into reflection type by depositing silver mirror at the fiber end face, which is highly sensitive to surrounding refractive index (RI). The GO nanosheets, as a two-dimensional hydrophilic nano material, is coated on the fiber surface, acting as a RH-to-RI converter. The simultaneous RH and temperature measurements are realized by monitoring the characteristic wavelength shifts of the SFT and FBG in the reflection spectrum. Experimental results show that the RH sensitivity of the probe is 161.1 pm/%RH during the range of 30%RH∼90%RH, and the temperature sensitivity is 14.1 pm/°C during the range of 10 °C∼50 °C. The proposed probe is compact, flexible, and easy to be fabricated, which has potential application for precise localized measurement in medical and biochemical fields.**

***Index Terms*—Optical fiber probe, S fiber taper, Graphene oxide, Fiber Bragg grating, Relative humidity measurement.**

I. Introduction

RELATIVE humidity (RH) sensors play an important role in the status monitoring of dangerous goods, building materials and biochemical process. In recent years, various optical fiber RH sensors have been designed, owing to their small size, fast response, high sensitivity, anti-electromagnetic interference, and corrosion resistance. Many sensing structures for RH measurement have been reported, such as fiber grating [1]–[3], directional coupler [4], [5], microfiber resonator [6]–[9], fiber interferometer [10]–[14]. For example, G. Woyessa *et al.* proposed a polycarbonate (PC) based polymer optical fiber Bragg grating (FBG) that can realize RH sensing within the temperature range from 20 °C to 100 °C [2]. However, relative large temperature cross-sensitivity and low humidity sensitivity limit its practical application. J. Yang *et al.* demonstrated a gelatin coated side-polished in-fiber directional coupler by splicing a segment of side-polished single eccentric hole-assistant dual-core fiber between two single mode fibers [4]. In spite of the high RH sensitivity, this coupler-based RH sensor was restricted by a narrow measurement range. N. Irawati *et al.* presented a zinc oxide (ZnO) coated polymethyl methacrylate (PMMA) microfiber loop resonator nanostructure, which possesses small size sensing element [7]. However, the RH resolution of this microfiber resonator-based RH sensor is limited by its relative low RH sensitivity. Therefore, the interferometer-based sensors have attracted more attention, whose measurement sensitivity and range can be improved with flexible structures, including Mach-Zehnder interferometers (MZIs), Sagnac interferometers and Fabry-Perot (FP) interferometers. Recently, S fiber taper (SFT) were widely studied as a key sensing element to measure refractive index (RI), force, and temperature [15]–[17]. When the light propagates in the SFT with two microbends, the cladding modes are excited at the first microbend owing to the excessive bending radius, and then the excited cladding modes are partly recoupled back into the core at the second microbend. Therefore, the SFT with surface evanescent field can be considered as a compact in-line MZI for sensing due to its advantages of small size, easy fabrication and high sensitivity. Y. Zhao *et al.* proposed a SFT based RH sensor by an in-situ layer-by-layer technique [13], the temperature fluctuations had less than 2%RH impact on the humidity test during the range of 30 °C∼45 °C. However, in the limited temperature range of 15 °C, the temperature-cross sensitivity is unsolved in fact, and the SFT based RH sensor works under the conventional transmission mode, which is limited in the measuring environment with special narrow space. Moreover, the transmission-type sensor with long size is easily disturbed by fiber bending, especially for the SFT with high strain-sensitivity [18].

Temperature cross sensitivity is a significant parameter that needs to be considered for RH sensors. In addition, RH is closely linked with temperature change because the saturated water vapor pressure in a sealed system changes with the variation

Manuscript received October 25, 2021; revised December 1, 2021; accepted December 15, 2021. Date of publication December 20, 2021; date of current version December 29, 2021. This work was supported in part by the National Natural Science Foundation of China under Grant 61735011, in part by the State Key Laboratory of Information Photonics and Optical Communications under Grant 2021KFKT006, in part by the Tianjin Talent Development Special Plan for High Level Innovation and Entrepreneurship Team, and in part by the first rank of Tianjin 131 Innovation Talent Development Program *(Zhankun Lv and Panpan Niu contributed equally to this work.) (Corresponding author: Junfeng Jiang).*

The authors are with the School of Precision Instrument and Opto-electronics Engineering, Tianjin University, Tianjin 300072, China, with the Key Laboratory of Opto-electronics Information Technology, Tianjin University, Tianjin 300072, China, and also with the Ministry of Education and Tianjin Optical Fiber Sensing Engineering Center, Institute of Optical Fiber Sensing of Tianjin University, Tianjin 300072, China (e-mail: lvzhankun@tju.edu.cn; niupanpan@tju.edu.cn; jiangjfjxu@tju.edu.cn; shuangwang@tju.edu.cn; lyzdoing@tju.edu.cn; tgliu@tju.edu.cn).

Digital Object Identifier 10.1109/JPHOT.2021.3136677

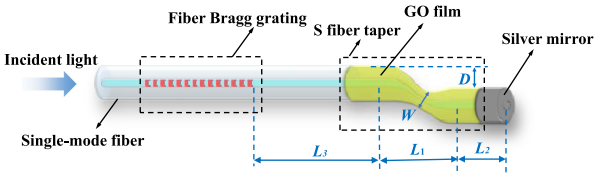

Fig. 1. Schematic diagram of the hybrid FBG/SFT structure probe.

of the environmental temperature. Therefore, the RH sensing makes sense only if the temperature information is provided at the same time. In order to compensate temperature cross sensitivity and detect temperature information, many hybrid structures have been proposed, such as FBG cascaded with FP cavity [19], FBG cascaded with up-tapered MZI [20], and FBG cascaded with tapered multi-mode fiber [21]. In order to adapt to the monitoring of a narrower environment, such as a microbial culture container, we have further compressed the size of the humidity sensor element.

In this paper, a reflective SFT-FBG hybrid structure is proposed for simultaneous measurement of RH and temperature. Graphene oxide (GO) nanosheets are deposited on the SFT surface as a RH-to-RI converter thanks to their unique hydrophilicity and large surface area [22], [23]. Silver coating is deposited on the SFT end face to make SFT work under reflection. FBG is located at the front of SFT for temperature sensing. The RH and temperature can be obtained simultaneously through measuring reflection spectrum with matrix calculation. The proposed optical fiber probe provides a linear and low hysteresis response in the range of 30%RH∼90%RH with sensitivity of 161.1 pm/%RH. Small footprint and single-end operation mode make the probe to be suitable for applications in medical and biochemical fields.

II. Probe Working Principle and Fabrication

Fig. 1 shows the schematic diagram of the proposed optical fiber probe for simultaneously measuring RH and temperature. The probe consists of an FBG and a reflective SFT with GO film. FBG is located at a distance of L_3 to the upstream of SFT to obtain temperature information. FBG is insensitive to RH due to its only usage of fiber core mode and is sensitive to ambient temperature through the intrinsic thermal expansion and thermal-optic effects of optical fiber core. SFT was fabricated by using a commercial fusion splicer (S178A, FITEL) with a particular splicing condition. *W*, L_1, *D* are the waist diameter, length and axial offset of the SFT respectively. Silver coating is deposited on the end face of the probe, L_2 away from the SFT. The hydrophilic material GO nanosheet is coated on the surface of the SFT, acting as a RH-to-RI converter. When the RH level rises, GO nanosheet layer adsorbs water molecules, thus the refractive index of the GO film will increase [24].

When light transmits in the SFT and is reflected by silver mirror, mutual coupling between core mode and cladding modes will happen at the two microbends, which means several transmission paths exist for both core mode and cladding modes. Cladding modes are sensitive to surrounding environment RI, therefore the interference can realize the RI sensing. The interference AC term of the reflective SFT spectrum can be described as [25], [26]

$$\begin{aligned} I_{AC} = {} & a_1 \cos(\Delta\Phi_1) + a_2 \cos 2(\Delta\Phi_2) + a_3 \cos 2(\Delta\Phi_1) \\ & + a_4 \cos 2(\Delta\Phi_1 + \Delta\Phi_2) + a_5 \cos(\Delta\Phi_1 + 2\Delta\Phi_2) \\ & + a_6 \cos(\Delta\Phi_1 - 2\Delta\Phi_2) \end{aligned} \tag{1}$$

$$\Delta\Phi_1 = \frac{2\pi\Delta_{neff}L_{eff}}{\lambda} \tag{2}$$

$$\Delta\Phi_2 = \frac{2\pi\Delta_{neff}L_2}{\lambda} \tag{3}$$

where $a_1 = 2\sqrt{I_{core}I_{cladding1}}$, $a_2 = 2\sqrt{I_{core}I_{cladding3}}$, $a_3 = 2\sqrt{I_{cladding2}I_{cladding3}}$, $a_4 = 2\sqrt{I_{core}I_{cladding2}}$, $a_5 = 2\sqrt{I_{cladding1}I_{cladding2}}$, $a_6 = 2\sqrt{I_{cladding1}I_{cladding3}}$. I_{core} is the intensity of the mode that transmits straightly in the core. $I_{cladding1}$ is the intensity of the modes excited at one microbend and coupled back to the core at the other microbend. $I_{cladding2}$ is the intensity of cladding modes excited at the first microbend and recoupled back to the core at the first microbend after being reflected by the silver mirror. $I_{cladding3}$ is the intensity of cladding modes excited at the second microbend and recoupled back to the core at the second microbend after being reflected by the silver mirror. $\Delta\Phi_1$ is the phase difference caused by one-way transmission in SFT, and $\Delta\Phi_2$ is the phase difference caused by transmission from SFT to silver mirror. Δ_{neff} is the effective RI difference of the core and the cladding mode. L_{eff} is the effective optical path of SFT, and L_2 is the distance between the SFT and the silver mirror. λ is the input wavelength in vacuum. As shown in Eq. (1), the wavelength shift can be attributed to the change in RI of the fiber surface.

Since the SFT and FBG have different responses to the RH and temperature, simultaneous measurement can be achieved through measuring reflection spectrum with matrix calculation.

$$\begin{bmatrix} \Delta RH \\ \Delta T \end{bmatrix} = \frac{1}{D} \begin{bmatrix} K_{FBG}^{T} & -K_{SFT}^{T} \\ -K_{FBG}^{RH} & K_{SFT}^{RH} \end{bmatrix} \begin{bmatrix} \Delta\lambda_{SFT} \\ \Delta\lambda_{FBG} \end{bmatrix} \tag{4}$$

Where $D = K_{SFT}^{RH}K_{FBG}^{T} - K_{SFT}^{T}K_{FBG}^{RH}$, ΔRH and ΔT are the changes of ambient RH and temperature, $\Delta\lambda_{SFT}$ and $\Delta\lambda_{FBG}$ are the wavelength shifts of the SFT and the FBG. K_{SFT}^{RH} and K_{FBG}^{RH} are the RH sensitivity coefficients of SFT and FBG, and K_{SFT}^{T} and K_{FBG}^{T} are the temperature sensitivity coefficients of SFT and FBG.

To coat GO film on the surface of SFT, we used a method based on chemical bonding concomitant with physical adsorption. Fig. 2 shows the process of SFT surface functionalization and the process of GO nanosheets deposition [27]. Prior to coating the GO film, the organic contaminant on the surface of the SFT was removed by rinsing with acetone solution and deionized water thoroughly. Firstly, immersing the SFT into NaOH solution (1.0 M) for 1 h at room temperature to prepare alkaline-treated SFT through the reaction of hydroxylation, which enrich the number of silanol (Si-OH) groups on the fiber surface (Fig. 2(b)). After that the hydroxylated SFT was rinsed with ethanol and deionized water for five times. Secondly, the fiber was immersed

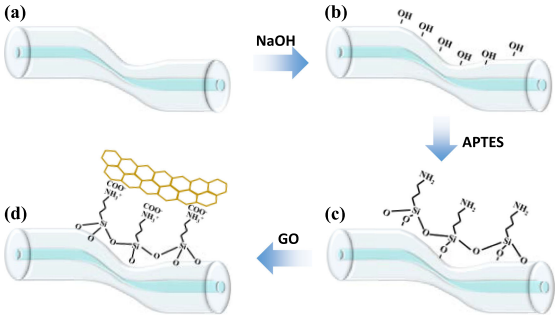

Fig. 2. Schematic diagram of the functionalization of the SFT surface and the deposition process of GO: (a) untreated SFT, (b) alkaline-treatment by NaOH, (c) silanization by APTES, (d) GO deposition.

into freshly-prepared 5% (V/V) 3-Aminopropyl triethoxysilane (APTES) for 1 h, which reacted with the hydroxyl groups to form Si-O-Si bonds. The silanized SFT was washed with ethanol and dried in a drying oven at 70 °C for 30 min, consolidating the stability of APTES monolayer (Fig. 2(c)). Finally, the fiber was immersed into 80 μg/mL diluted GO aqueous solution for 10 min. GO nanosheets were electrostatically adsorbed to the fiber surface with the volatilization of the aqueous, as a result of the reaction of the epoxy group in GO with the amino group in APTES (Fig. 2(d)). To remove the unbound GO nanosheets and consolidate the GO film, the GO-coated fiber was immersed into deionized water for 30 min, and dried in a drying oven at 50 °C for 1.5 h.

SFT end face was then chemically coating with silver through silver mirror reaction. The SFT end face was deoiled with acetone and ethanol 3 times and coarsened with 35% (V/V) hydrofluoric acid (HF) for 5 min, and sensibilizing with tin (ii) fluoride (2.0 g/L) for 5 min. After completion of pretreatments, the SFT end face is immersed into the solution composed of Tollen's reagent and potassium sodium tartrate (100 g/L) for 10 min. It should be noted that SFT micro-structure must not be immersed in the reaction solution.

Fig. 3 shows the fabricated probe. The geometry parameters L_1, D, W of the SFT are 673 μm, 97 μm and 45 μm respectively, as shown in Fig. 3(a). The distance between the silver mirror and the back end of the SFT L_2 was controlled to be $\sim$300μm. The distance between the SFT and the FBG L_3 was shortened to $\sim$1 mm for compactness. The length of the SFT-FBG hybrid probe is less than 13 mm. Fig. 3(b) showed the SEM image of the side view of the probe GO film. It can be seen that GO film had a uniform distribution. Fig. 3(c) illustrates that the coating thickness is $\sim$1.54 μm. Fig. 3(d) shows the silver mirror at the end of the probe.

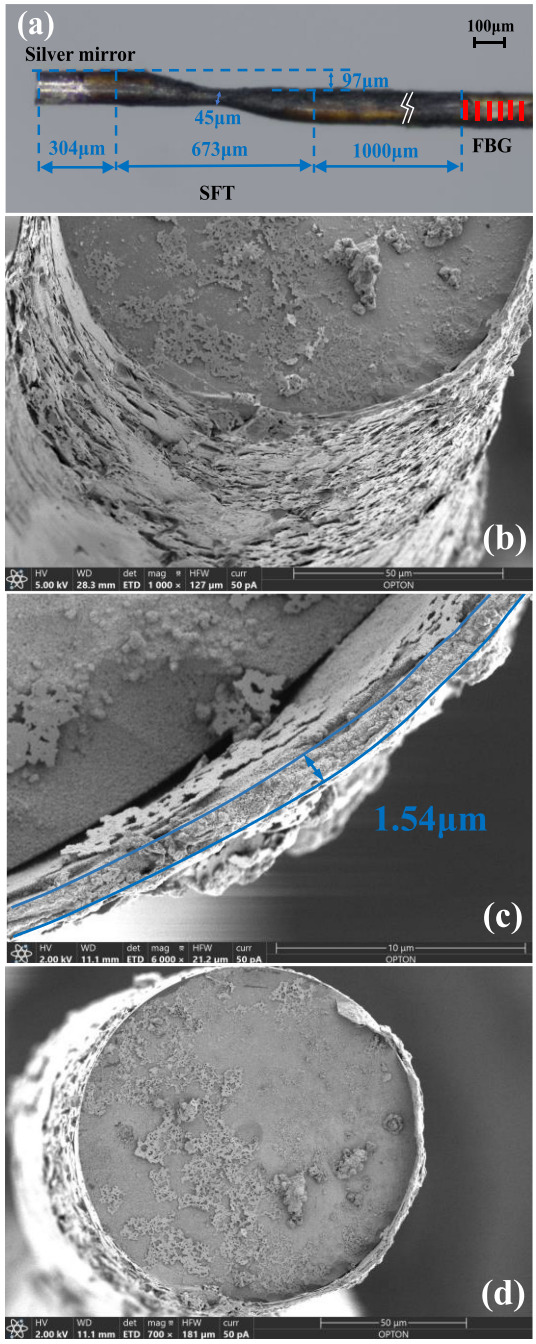

Fig. 3. (a) Micrograph of the prepared probe. (b) SEM image of the side view of the hybrid FBG/SFT structure probe. (c) SEM image of the SFT cross section. (d) SEM image of the silver mirror at the end face of the probe.

III. Experiment Results and Discussion

Fig. 4 is the experimental setup for RH and temperature measurement. In order to avoid disturbance caused by bending and strain, the sensing probe was mounted on a quartz slide surface by UV glue, and only one glue point was applied on the upstream single-mode fiber of FBG. Then the probe was placed into a temperature and humidity chamber with a resolution of 1%RH and 0.1 °C. The light from a broadband optical source (BBS) was injected into a 3-port optical circulator (Cir) through port 1, and the probe was connected to the port 2. The reflection spectrum was monitored by an optical spectrum analyzer (OSA) through port 3.

For the RH measurement, the RH of the chamber was set to rise from 30%RH to 90%RH with a step of 10%RH remaining a constant temperature of 30 °C, and the experimental RH range covers the main measurement in medical and manufacturing [28]. Fig. 5(a) shows the measured reflection spectrum evolution

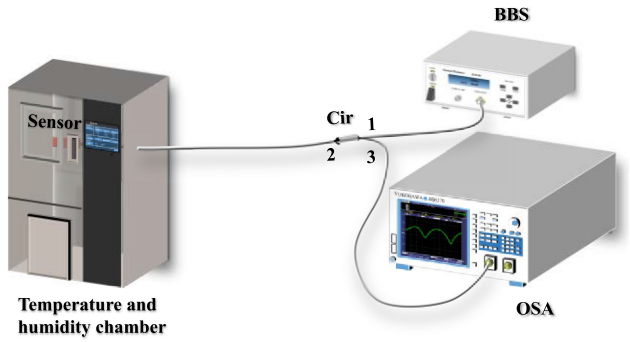

Fig. 4. Schematic diagram of the experimental setup for RH and temperature measurement.

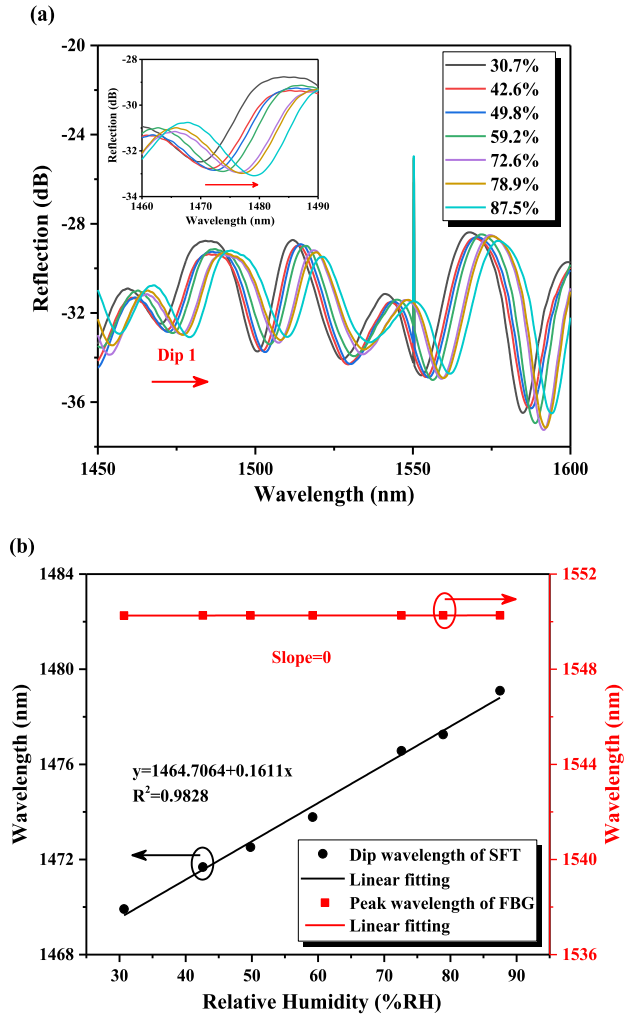

Fig. 5. (a) Reflection spectra of the FBG/SFT probe under different RHs in increasing order. (b) Wavelength responses of the SFT (black) and the FBG (red) under different RHs in increasing order.

of the probe under different RHs. It can be observed that as RH rises, the reflection spectrum of SFT has a redshift. The interference dip located at ∼1471 nm (Dip 1) was selected to characterize the wavelength response for RH measurement, which is far from that of FBG to avoid overlap. As shown in Fig. 5(b), in the range of 30.7%RH to 87.5%RH, dip 1 uplifts

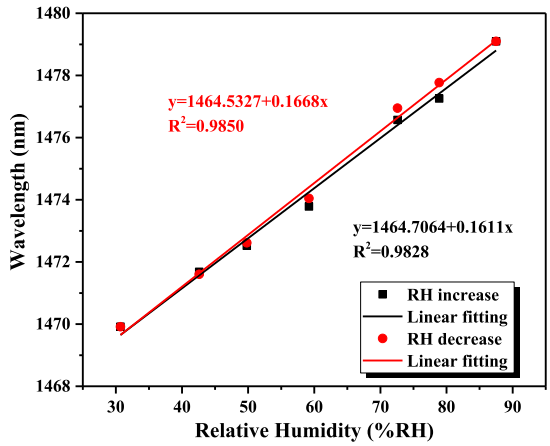

Fig. 6. Wavelength responses of the SFT under different RHs in both increasing and descending orders.

from 1469.914 nm to 1479.096 nm, with a 9.182 nm shift. The linear fitting result indicates that the wavelength variation of the Dip 1 assumed a good linear relationship with the RH and the R^2 value is 0.9828, and sensitivity is 161.1 pm/%RH. The wavelength of FBG remains stable as expected. The reflection spectrum was recorded in a descending RH for hysteresis test of the probe. As shown in the Fig. 6, for the probe tested in this work, the maximum hysteresis is <4%RH, and the hysteresis during high RH is attributed to the sorption/desorption interaction between the graphene oxide and the water molecules [29].

To measure the temperature response, the chamber was heated from 10 °C to 50 °C with an interval of 10 °C under a fixed RH of 30%RH. For thermal stability of the GO film, the temperature measuring range was controlled to be 10 °C∼50 °C [30]. The reflection spectrum was recorded in stable way by one hour waiting time at each settled temperature. Fig 7(a) shows the spectrum evolutions of the probe under different temperatures. As the environment temperature increases, the peak wavelength of FBG has a redshift. The inset of Fig. 7(a) shows the detail of the FBG wavelength shift. The fitting result in Fig. 7(b) indicates that the FBG wavelength shows a significant linear relationship to temperature, with a sensitivity of 14.1 pm/°C. Moreover, the reflection spectrum of the SFT has a blueshift with the sensitivity of −2.4 pm/°C. In the range of 40 °C, the temperature change had less than 1%RH influence on the RH measurement. The SFT provides a relative low temperature sensitivity. Thermal expansion effect causes axial deformation of SFT, which results in the blue shift of spectrum. While it is partially offset by the spectral red shift caused by the thermo-optic effect. Consequently, with the above achieved sensitivity coefficients, we can rewrite Eq. (4) as follow:

$$\begin{bmatrix} \Delta RH \\ \Delta T \end{bmatrix} = \frac{1}{2271.51} \begin{bmatrix} 14.1 & 2.4 \\ 0 & 161.1 \end{bmatrix} \begin{bmatrix} \Delta\lambda_{SFT} \\ \Delta\lambda_{FBG} \end{bmatrix} \quad (5)$$

Therefore, the RH and temperature information can be measured by calculating the sensor matrix through Eq. (5). Owing to the wavelength resolution of OSA is 0.02 nm, the RH sensing resolution of the probe is 0.145%RH.

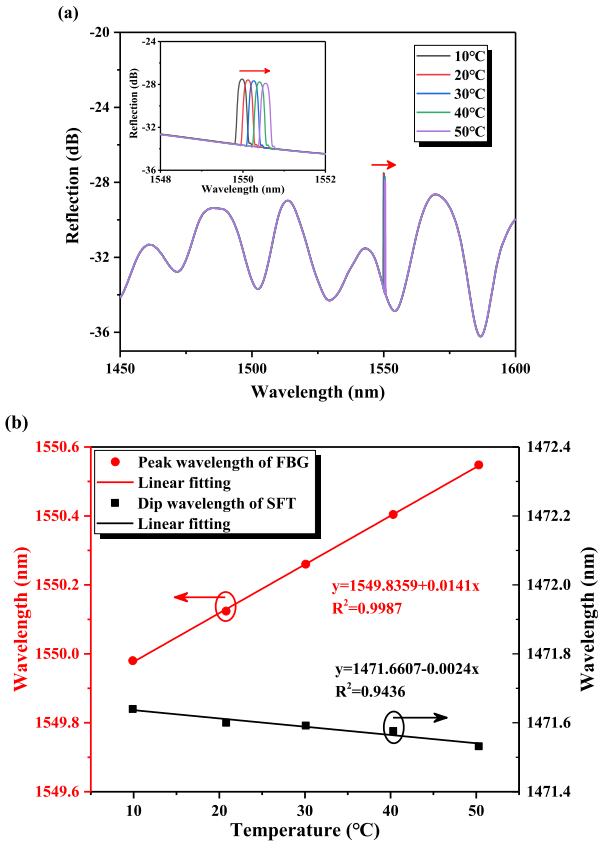

Fig. 7. (a) Reflection spectra of the FBG/SFT probe under different temperatures. (b) Wavelength responses of the FBG (red) and the SFT (black) under different temperatures.

To verify the capability of measuring RH and temperature simultaneously, the temperature and humidity variations were implemented to the probe at room environment with temperature of 26 °C and RH of 67%RH. When the temperature rises to 30 °C, the RH was set to increase from 30%RH to 90%RH with an interval of 10%RH. After a series of first round measurements, the sensing spectrum of probe was restored to the initial state at room environment, and the RH was changed to 60%RH, meanwhile the temperature was changed from 10 °C to 50 °C with an interval of 5 °C for second round measurements. By discriminating the wavelength shifts of the SFT and the FBG, the applied RH and temperature were demodulated with Eq. (5), and the demodulated results are shown in Fig. 8, which agree well with the applied values. The maximum deviations of RH and temperature measurement are only 2.9%RH and 0.4 °C, respectively. Experimental results illustrate that the designed probe could resolve the temperature cross-sensitivity for RH sensing, which is a promising platform for simultaneously measuring the RH and temperature.

Considering that it is already relatively common to measure temperature with FBG, we will not compare temperature sensing performance of the probe here. The RH sensing performance comparison of different GO-based optical fiber RH sensors are listed in Table I. The table shows that in a wide RH range our proposed probe has a high sensitivity with an good linearity, meanwhile the size of the RH sensing element was compacted.

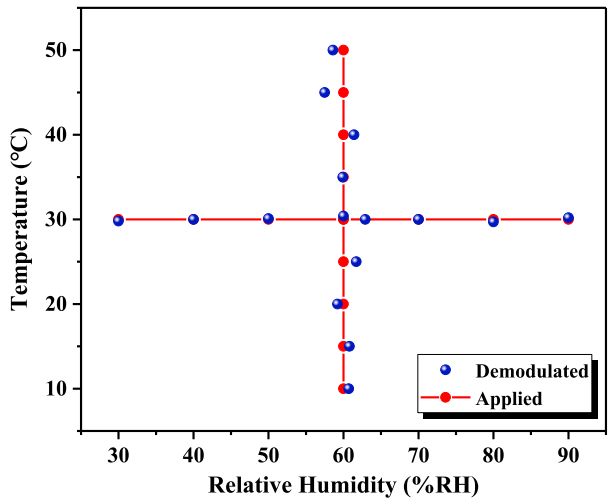

Fig. 8. Demodulated results calculated by Eq. (5) under the applied RH and temperature simultaneously.

TABLE I
RH SENSING PERFORMANCE OF DIFFERENT GO-BASED OPTICAL FIBER SENSORS

Fiber structure	Sensing range (%RH)	Sensitivity (nm/%RH)	Sensing element size (mm)	Temperature cross-sensitivity	Reference
Tilted fiber grating	30~80	0.0185	15	Unsolved	[3]
Microfiber-Knot resonator	0~80	0.0104	0.00302	Unsolved	[9]
Hollow core fiber	13.47~81.34	0.11725	--	Unsolved	[11]
Up-tapered MZI	9.73~80.37	0.0061	30	Unsolved	[20]
Corroded fiber MZI	30~55 55~95	0.191 0.061	30	Unsolved	[10]
SFT	44~95	0.284	0.822	Unsolved	[13]
SFT-FBG	30~90	0.1611	0.673	Resolved	This paper

In addition, the probe shows the advantages of easy fabrication and low cost, which make it potential applied in medical and biochemical fields, such as precise localized monitoring of the process of cell culture.

IV. CONCLUSION

In conclusion we have experimentally demonstrated the proposed optical fiber probe based on a FBG cascaded to the upstream of a reflective SFT with GO film for measuring RH and temperature simultaneously. Experimental results show that the RH sensitivity is 161.1 pm/%RH during the range of 30%RH~90%RH, and the temperature sensitivity is 14.1 pm/°C, ranging from 10 °C to 50 °C. Moreover, the probe performed good reversibility and accuracy during experiment.

Due to the compact structure and reflective detection, the proposed probe is a promising alternative for simultaneous RH and temperature measurement in medical and biochemical fields.

REFERENCES

[1] L. W. Wang, Y. Liu, M. Zhang, D. S. Tu, X. H. Mao, and Y. B. Liao, "A relative humidity sensor using a hydrogel-coated long period grating," *Meas. Sci. Technol.*, vol. 18, no. 10, pp. 3131–3134, Oct. 2007, doi: 10.1088/0957-0233/18/10/S13.

[2] G. Woyessa, A. Fasano, C. Markos, H. K. Rasmussen, and O. Bang, "Low loss polycarbonate polymer optical fiber for high temperature FBG humidity sensing," *IEEE Photon. Technol. Lett.*, vol. 29, no. 7, pp. 575–578, Apr. 2017, doi: 10.1109/LPT.2017.2668524.

[3] B. Jiang *et al.*, "Graphene oxide-deposited tilted fiber grating for ultrafast humidity sensing and human breath monitoring," *Sensors Actuators B Chem.*, vol. 293, pp. 336–341, Aug. 2019, doi: 10.1016/j.snb.2019.05.024.

[4] J. Yang *et al.*, "High sensitivity humidity sensor based on gelatin coated side-polished in-fiber directional coupler," *Sensors Actuators B Chem.*, vol. 305, Feb. 2020, Art. no. 127555, doi: 10.1016/j.snb.2019.127555.

[5] L. Bo, P. Wang, Y. Semenova, and G. Farrell, "Optical microfiber coupler based humidity sensor with a polyethylene oxide coating," *Microw. Opt. Technol. Lett.*, vol. 57, no. 2, pp. 457–460, Feb. 2015, doi: 10.1002/mop.28874.

[6] N. Irawati, H. A. Rahman, H. Ahmad, and S. W. Harun, "A PMMA microfiber loop resonator based humidity sensor with ZnO nanorods coating," *Measurement*, vol. 99, pp. 128–133, Mar. 2017, doi: 10.1016/j.measurement.2016.12.021.

[7] N. Irawati, T. N. R. Abdullan, H. A. Rahman, H. Ahmad, and S. W. Harun, "PMMA microfiber loop resonator for humidity sensor," *Sensors Actuators A Phys.*, vol. 260, pp. 112–116, Jun. 2017, doi: 10.1016/j.sna.2017.04.041.

[8] J. C. Shin, M.-S. Yoon, and Y.-G. Han, "Relative humidity sensor based on an optical microfiber knot resonator with a polyvinyl alcohol overlay," *J. Lightw. Technol.*, vol. 34, no. 19, pp. 4511–4515, Oct. 2016, doi: 10.1109/JLT.2016.2552494.

[9] S. R. Azzuhri *et al.*, "Application of graphene oxide based microfiber-knot resonator for relative humidity sensing," *Results Phys.*, vol. 9, pp. 1572–1577, Jun. 2018, doi: 10.1016/j.rinp.2018.05.009.

[10] X. Fan *et al.*, "Humidity sensor based on a graphene oxide-coated few-mode fiber Mach-Zehnder interferometer," *Opt. Exp.*, vol. 28, no. 17, pp. 24682–24692, Aug. 2020, doi: 10.1364/OE.390207.

[11] Y. Zhao, R.-J. Tong, M.-Q. Chen, and F. Xia, "Relative humidity sensor based on hollow core fiber filled with GQDs-PVA," *Sensors Actuators B Chem.*, vol. 284, pp. 96–102, Apr. 2019, doi: 10.1016/j.snb.2018.12.130.

[12] N. Chen, X. Zhou, and X. Li, "Highly sensitive humidity sensor with low-temperature cross-sensitivity based on a polyvinyl alcohol coating tapered fiber," *IEEE Trans. Instrum. Meas.*, vol. 70, pp. 1–8, 2021, Art. no. 9503308, doi: 10.1109/TIM.2020.3034154.

[13] Y. Zhao *et al.*, "Relative humidity sensor of S fiber taper based on graphene oxide film," *Opt. Commun.*, vol. 450, pp. 147–154, Nov. 2019, doi: 10.1016/j.optcom.2019.05.072.

[14] M.-Q. Chen, Y. Zhao, H.-M. Wei, C. L. Zhu, and S. Krishnaswamy, "3D printed castle style Fabry-Perot microcavity on optical fiber tip as a highly sensitive humidity sensor," *Sensors Actuators B Chem.*, vol. 328, Feb. 2021, Art. no. 128981, doi: 10.1016/j.snb.2020.128981.

[15] P. Niu, J. Zhao, C. Zhang, H. Bai, X. Sun, and J. Bai, "Reflective intensity-demodulated refractometer based on S fiber taper," *IEEE Photon. Technol. Lett.*, vol. 30, no. 1, pp. 55–58, Jan. 2018, doi: 10.1109/LPT.2017.2773638.

[16] J. Li *et al.*, "Simultaneous force and temperature measurement using S fiber taper in fiber Bragg grating," *IEEE Photon. Technol. Lett.*, vol. 26, no. 3, pp. 309–312, Feb. 2014, doi: 10.1109/LPT.2013.2293132.

[17] J. Zhao, P. Niu, C. Zhang, X. Sun, H. Bai, and C. Miao, "Temperature-compensated fiber laser refractometer based on compact hybrid S-taper/FBG structure," *Opt. Fiber Technol.*, vol. 45, pp. 300–305, Nov. 2018, doi: 10.1016/j.yofte.2018.08.006.

[18] J. Zhang *et al.*, "Bending vector sensor based on Mach-Zehnder interferometer using S type fibre taper and lateral-offset," *J. Modern Opt.*, vol. 63, no. 21, pp. 2146–2150, 2016, doi: 10.1080/09500340.2016.1185177.

[19] Y. F. Qi, C. Jia, L. Tang, M. J. Wang, Z. M. Liu, and Y. Y. Liu, "Simultaneous measurement of temperature and humidity based on FBG-FP cavity," *Opt. Commun.*, vol. 452, pp. 25–30, Dec. 2019, doi: 10.1016/j.optcom.2019.07.014.

[20] R. J. Tong, Y. Zhao, M. Q. Chen, X. G. Hu, and Y. Yang, "Simultaneous measurement of RH and temperature based on FBG and balloon-like sensing structure with inner embedded up-tapered MZI," *Measurement*, vol. 146, pp. 1–8, Nov. 2019, doi: 10.1016/j.measurement.2019.06.018.

[21] J. Z. Li *et al.*, "An optical fiber sensor coated with electrospinning polyvinyl alcohol/carbon nanotubes composite film," *Sensors*, vol. 20, no. 23, Dec. 2020, Art. no. 6996, doi: 10.3390/s20236996.

[22] D. R. Dreyer, S. Park, C. W. Bielawski, and R. S. Ruoff, "The chemistry of graphene oxide," *Chem. Soc. Rev.*, vol. 39, no. 1, pp. 228–240, 2010, doi: 10.1039/b917103g.

[23] Y. Yao, X. Chen, J. Zhu, B. Zeng, Z. Wu, and X. Li, "The effect of ambient humidity on the electrical properties of graphene oxide films," *Nanoscale Res. Lett.*, vol. 7, pp. 1–7, Jul. 2012, Art. no. 363, doi: 10.1186/1556-276X-7-363.

[24] O. Leenaerts, B. Partoens, and F. M. Peeters, "Adsorption of H_2O, NH_3, Co, No_2, and NO on graphene: A first-principles study," *Phys. Rev. B*, vol. 77, no. 12, Mar. 2008, Art no. 125416, doi: 10.1103/PhysRevB.77.125416.

[25] P. Lu *et al.*, "Tapered fiber Mach–Zehnder interferometer for simultaneous measurement of refractive index and temperature," *Appl. Phys. Lett.*, vol. 94, Art. no. 131110, 2009, doi: 10.1063/1.3115029.

[26] Q. Wang *et al.*, "Optimization of cascaded fiber tapered Mach–Zehnder interferometer and refractive index sensing technolog," *Sensors Actuators B Chem.*, vol. 222, pp. 159–165, 2016, doi: 10.1016/j.snb.2015.07.098.

[27] C. Liu *et al.*, "Graphene oxide functionalized long period grating for ultrasensitive label-free immunosensing," *Biosensors Bioelectron.*, vol. 94, pp. 200–206, Aug. 2017, doi: 10.1016/j.bios.2017.03.004.

[28] R. Fenner and E. Zdankiewicz, "Micromachined water vapor sensors: A review of sensing technologies," *IEEE Sensors J.*, vol. 1, no. 4, pp. 309–317, Dec. 2001, doi: 10.1109/7361.983470.

[29] E. U. Park *et al.*, "Correlation between the sensitivity and the hysteresis of humidity sensors based on graphene oxides," *Sensors Actuators B Chem.*, vol. 258, pp. 255–262, Apr. 2018, doi: 10.1016/j.snb.2017.11.104.

[30] P. G. Ren *et al.*, "Temperature dependence of graphene oxide reduced by hydrazine hydrate," *Nanotechnology*, vol. 22, no. 5, 2010, Art. no. 055705, doi: 10.1088/0957-4484/22/5/055705.